Electronic Supplementary Information

All-ceramic asymmetric membranes with superior hydrogen permeation

Daniel Montaleone, Elisa Mercadelli*, Sonia Escolástico, Angela Gondolini, José M. Serra,

Alessandra Sanson

1. Experimental

1.1 Membrane fabrication and microstructural characterization

The steps of the process used for the membrane fabrication, are schematized in Figure S.1.

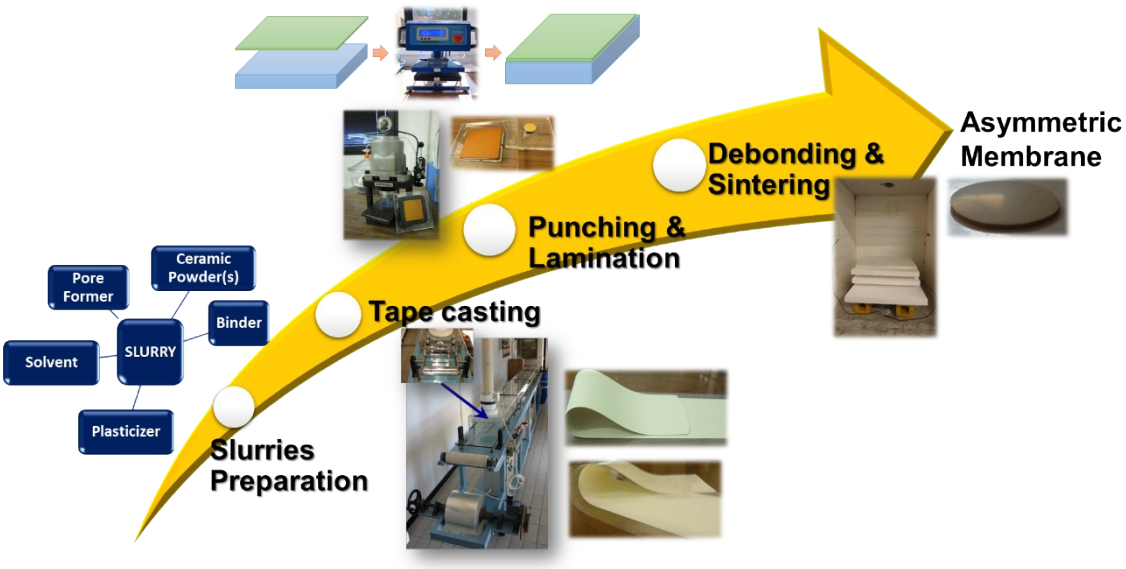

Figure S.1 Schematic representation of the production of the slurry for the membrane layer.

For the production of the porous substrate, BCZY ($BaCe_{0.65}Zr_{0.20}Y_{0.15}O_{3-\delta}$, Specific Surface Area (SSA) = 5.8 m^2/g), supplied by Marion Technology and GDC powders ($Gd_{0.2}Ce_{0.8}O_{2-\delta}$, SSA = 6.8 m^2/g, supplied by FuelCellMaterials in a ratio equal to 50/50 vol %, were used as starting material. Rice Starch (RS, Fluka, Germany), with average particle size of 5-6 μm was used as sacrificial pore forming agent. The amount of pore former was fixed at 40 vol.% respects to the BCZY powders.

On the other hand, BCZY (SSA = 12.2 m^2/g, supplied by Marion Technology) and GDC powders in a ratio equal to 50/50 vol % were used for the production of the dense membrane. ZnO (Sigma Aldrich) was directly

added into the tape casting suspension to promote the membrane densification. The total amount of the sintering aid was fixed at 1 wt %.[1]

The slurries were prepared following the procedure already described in a previous work.[2] The composition of the green supporting substrate and of the dense membrane are reported in Table S1.

Table S.1 Composition of the green tape for the production of the porous supporting substrate and of the dense membrane.

	Supporting substrate	**Dense membrane**
Component	***(Vol %)***	***(Vol %)***
Ceramic powder (BCZY+GDC)	23.4	38.3
Pore former	26.9	/
Deflocculant	1.5	4.1
Binder	23.0	29.1
Plasticizer	25.2	28.5

The green tapes were punched in discs of 24 mm in diameter. An uniaxial warm press was used to laminate the green tape layers to produce the asymmetrical BCZY-GDC bilayers. The two discs were stacked between polished parallel steel plates and heated at 55°C applying applying a pressure of 0.7 bar.

The bilayers were finally debinded and sintered at 1500 °C for four hours. Two different powder systems were used as sources of barium during sintering: BCZY and a 50/50 vol% mixture of BCZY-GDC following the experimental set-up already reported in a recent work.[3]

The microstructure of the sintered membranes was investigated by scanning electron microscopy (SEM-FEG, Carl Zeiss Sigma NTS GmbH, Oberkochen, Germany), embedding the cross sections under vacuum in epoxy resin and then polishing them down to 0.25 μm finish. Ba-, Ce- and Gd-element concentration profiles were recorded using the EDS probe (EDS, X-Act, INCA Energy 300, Oxford Instruments, Abingdon, UK) to assess the distribution of the BCZY and GDC phases.

To check the composition of the cer-cer membrane layer, XRD analyses were performed on the dense surface at room temperature using a Bruker D8 Advance diffractometer (Bruker AXS GmbH, Karlsruhe, Germany) on a Bragg-Brentano geometry with an X-ray tube operating at 40 kV and 40 mA. Data were collected through a one-dimensional LynkEye detector based on silicon strip technology, set to discriminate Cu Kα1,2 radiation, in the 10-80° 2θ measuring range, with an equivalent counting time of 10s per 0.02° 2θ step anode X-ray. Phase analysis of XRD collected data were performed by means of HighScore Plus v.3.0 (PANalytical B. V.,

Almelo, The Netherlands). EXPGUI v.1208 interface [4] for the GSAS [5] was used to achieved quantitative phases analysis and unit-cell parameters perovskite main phase from X-ray diffraction data.

The residual porosity of the active membrane layer was determined by image analysis of the polished cross-sections using the software ImageJ while the porosity of the porous substrate was evaluated by Hg intrusion (Pascal 140 and 240 series, Thermo Finnigan, Waltham, MA, USA).

1.2 Hydrogen permeation measurements

Permeation measurements were performed on a double chamber quartz reactor following the procedure previously reported. [6,7] Argon was used on the permeate side as sweep gas (150 mL·min^{-1}) whereas a mixture of H_2-He (100 mL·min^{-1}) was fed to the retentate side. Measurements were performed with the membrane layer and the support on the feed and the sweep side, respectively. Sealing was accomplished using a silver based alloy ring.

Permeation measurements were performed under three hydration degree configurations: (A) feed side humidified (pH_2O = 0.025 atm); (B) both membrane sides humidified (pH_2O=0.025 atm); and (C) sweep side humidified (pH_2O = 0.025 atm). The H_2 content in the permeate side was analyzed using a micro-GC Varian CP-4900 equipped with Molsieve5A and PoraPlot-Q glass capillary modules. He was also continuously monitored to evaluate the leaks in the system. GC analyses were performed after 30 minutes of stabilization in the steady state and each condition was analyzed three times. H_2 fluxes (mL·min^{-1}·cm^{-2}) were calculated at standard conditions.

2. Post-mortem membranes characterization

After permeation measurements, the membranes were investigated through SEM and XRD analyses in order to assess any morphological and/or compositional modifications. Figure S.2 (a) and (b) shows the SEM micrographs of the single-phase membrane fresh and polished cross section respectively, while the backscattered image of the polished section and the corresponding EDS scanlines for Ce, Ba and Gd of the same membrane are reported in Figure S.2 (c) and (d). Comparing the microstructural characterization of the as-sintered single phase membrane (Fig 1) with the post-mortem results, it is evident that no apparent morphological and compositional alterations occurred during permeation tests. The cracks detected onto the polished cross sections of the membrane (Fig S.2 b and c) were caused by the polishing treatment. No cracks were in fact discernible into the fresh cross section of the same membrane.

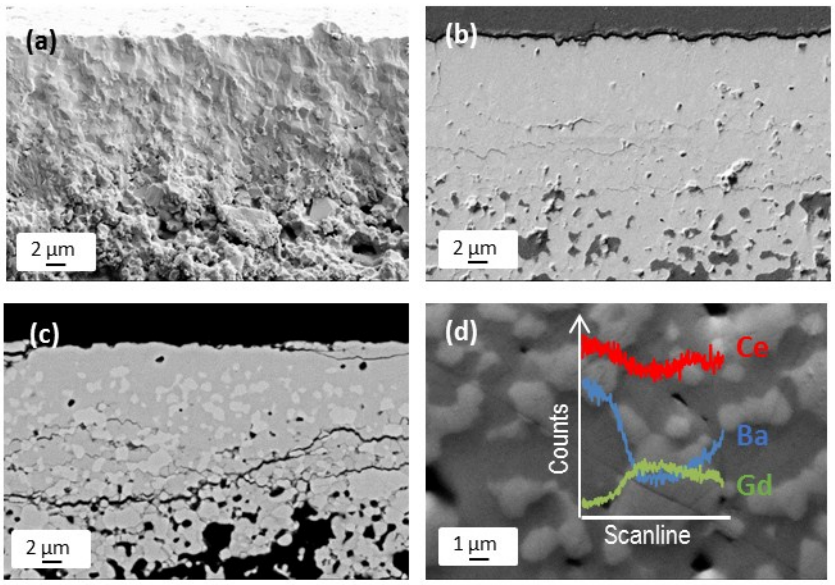

Figure S.2 SEM micrographs of the fresh cross section (a), the secondary electron image (b) and the backscattered image (c) of the polished cross section of the "single phase" asymmetric membrane post mortem. EDS scanlines of the central part of the cer-cer dense layer polished cross section (d).

Figure S.3 shows the SEM micrographs of the polished and fresh cross section of the "double phase membrane". Figure S.3 (d) depicts the EDS scanlines for the polished cross section of the dense membrane layer.

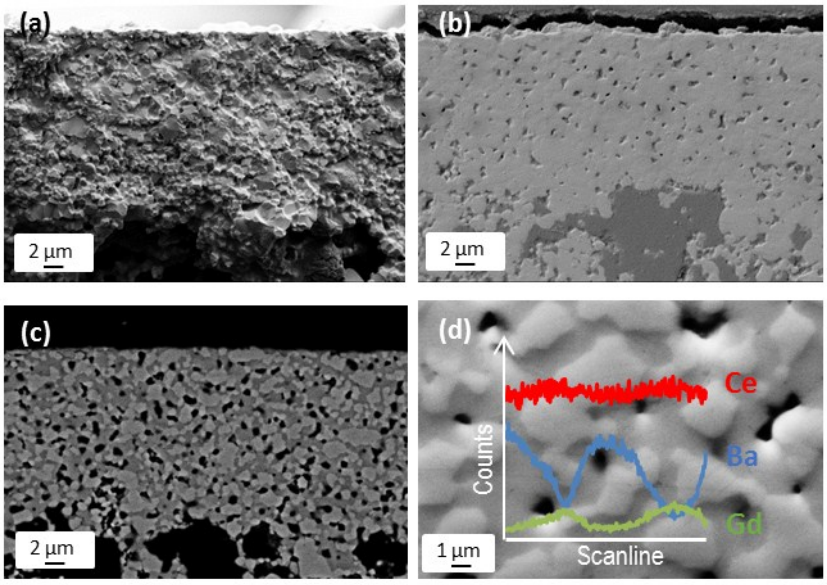

Figure S.3 SEM micrographs of the fresh cross section (a), the secondary electron image (b) and the backscattered image (c) of the polished cross section of the "double phase" asymmetric membrane post mortem. EDS scanlines of the central part of the cer-cer dense layer polished cross section (d).

.

Also in this case, no morphological and/or compositional changes can be detected comparing the microstructural characterization of the as-sintered membrane (Fig. 3) with the SEM-EDS results of the post-mortem membrane. No interdiffusion was in fact registered during permeation tests, while the shape and the morphology of the BCZY and GDC grains remained unchanged.

The XRD analyses carried out on the dense top surface membranes (Figure S.4) confirmed that the phase composition of the single and double phase membrane was not modified, and no apparition of secondary phases were detected.

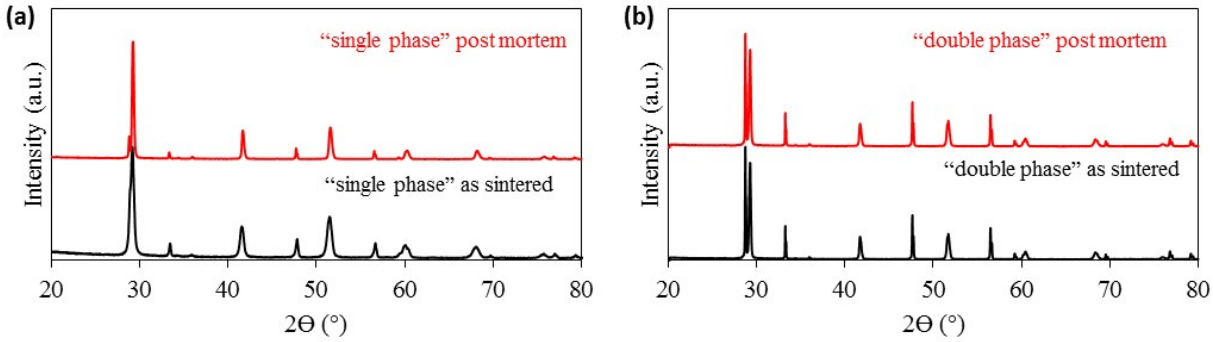

Figure S.4 XRD pattern of the "single phase" membrane **(**a) and the "double phase" membrane (b) as sintered and post mortem.

Finally, the SEM micrographs of the fresh fracture depicted in Figure S.5 showed that the Pt nanoparticles maintained their morphology and distribution through the BCZY-GDC porous support.

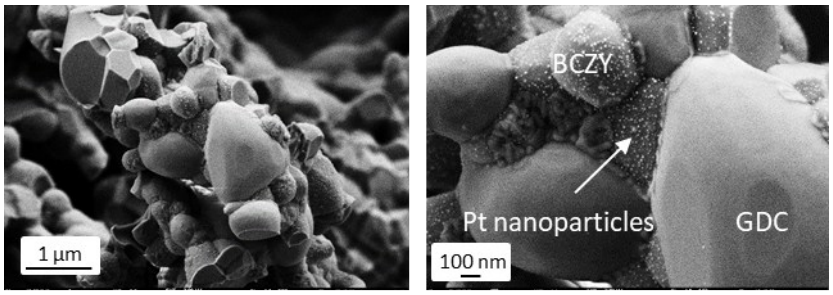

Figure S.5 SEM micrographs of the fresh fracture of the Pt activated porous support after permeation measurements.

References

1 Y. Li, R. Guo, C. Wang, Y. Liu, Z. Shao, J. An, C. Liu, *Electrochim. Acta*, 2013, **95**, 95-101.

2 E. Mercadelli, D. Montaleone, A. Gondolini, P. Pinasco, A. Sanson, *Ceram. Int.*, 2017, **43**, 8010-8017.

3 D. Montaleone, E. Mercadelli, A. Gondolini, M. Ardit, P. Pinasco, A. Sanson, *J. Eur. Ceram Soc.*, 2018, DOI: https://doi.org/10.1016/j.jeurceramsoc.2018.01.043

4 B. H. Toby, *J. Appl. Crystallogr*., 2001, **34**, 210-213.

5 A. C. Larson., R. B. Von Dreele, *Los Alamos National Laboratory Report LAUR,* 2004, 86-748.

6 S. Escolástico, C. Solís, C. Kjølseth, J.M. Serra, *ACS Applied Materials & Interfaces*, 2017, **9** (41), 35749-35756

7 S. Escolástico, S. Somacescu, J. M. Serra, *J. Mater. Chem. A*, 2015, **3**(2), 719-731.